Fatigue & Fracture of Engineering Materials & Structures

WILEY

FFEMS Fatigue & Fracture of Engineering Materials & Structures

ORIGINAL ARTICLE OPEN ACCESS

On the Identification of Dissipative Phenomena in Fatigue-Loaded 2024 Aluminum by Means of Second Harmonic of Temperature Analysis

Riccardo Cappello[1,2] | José Eugénio Semedo Garção[3] | Giuseppe Catalanotti[3,4] | Giuseppe Pitarresi[1]

[1]Department of Engineering, University of Palermo, Palermo, Italy | [2]Bristol Composites Institute, School of Civil, Aerospace and Design Engineering, University of Bristol, Bristol, UK | [3]Escola de Ciências e Tecnologia, Universidade de Évora, Évora, Portugal | [4]Department of Engineering, Kore University of Enna (UKE), Enna, Italy

Correspondence: Riccardo Cappello (riccardo.cappello@bristol.ac.uk)

Received: 21 March 2025 | **Revised:** 19 May 2025 | **Accepted:** 7 June 2025

Funding: The first author acknowledges the support of the EPSRC Programme Grant "Certification for Design–Reshaping the Testing Pyramid" (CerTest, EP/S017038/1). The signal processing methodology presented was developed with the support of the European Union's Framework Program for Research and Innovation – Mission 4 – Component C2 Investment 1.1 (PRIN-2022) – project title MAdforLIFE, code: 2022JE3LRA_001, CUP: B53D23006070006.

Keywords: aluminum | dissipation | fatigue | infrared thermography | thermoelastic stress analysis

ABSTRACT

This study explores the use of temperature harmonics to detect intrinsic dissipation during cyclic loading in aluminum alloys. Under sinusoidal loading, the temperature of a solid is modulated by thermomechanical heat sources. The primary source is the thermoelastic effect, which modulates the temperature at the load frequency and twice the load frequency (second harmonic). Thermoelastic stress analysis (TSA) signal processing is employed to extract the temperature harmonics and analyze their evolution when the stress amplitude increases. The detected second harmonic comprises three main contributions: a thermoelastic component, predicted by the second-order thermoelastic effect theory, a spurious contribution due to load components at twice the nominal frequency, and a dissipative second harmonic. The main aim of this work is to separate the thermoelastic and spurious contributions from the measured second harmonic to isolate and capture dissipation. AL 2024 alloy samples, which exhibits strong second-order thermoelastic response, are employed in the investigation. Aluminum has already been reported as a material where thermomechanical dissipation is difficult to quantify, or even qualitatively observe, with other more traditional thermographic methods. The results show interesting features of the second-harmonic decoupled components, providing insight into intrinsic dissipation of aluminum alloys under fatigue-loading conditions.

1 | Introduction

Evaluating changes in the structural health of materials and structures using infrared thermography (IRT) has become a concrete and appealing practice due to notable progress in infrared hardware and digital signal processing technologies. A critical factor in harnessing such technological potential is the capacity to correlate the mechanical behavior with the temperature field measurable on the structure's surface [1–3]. This requires a comprehensive understanding of the thermomechanical sources under various loading conditions and the associated energy dissipation and heat transfer. A particularly focused area of research pertains to the behavior of materials under cyclic loading characteristic of fatigue regimes. The objective of thermographic methods in this context is to correlate temperature-based metrics to the material irreversible changes induced by fatigue loading. During the last 25 years, considerable effort has been spent in the tentative development

Summary

- A novel framework isolates dissipative phenomena in the temperature second harmonic.
- Application to AL 2024 T3 confirms weak dissipation and strong second-order thermoelasticity.
- Dissipation signs emerge in the second harmonic of the load signal.
- The approach advances thermography for metals with strong higher order thermoelastic effects.

of a thermographic procedure to rapidly determine the fatigue performances of metallic materials using infrared thermography. This has resulted in a wealth of approaches and methods recently comprehensively reviewed in a few articles [4–7]. The central aim of these studies is the development of a *fatigue thermographic method*, and more specifically a *fatigue limit thermographic method* (FLTM). Most of such works are based on applying the so-called stepwise testing approach [2, 8–28]. This consists of loading tensile samples at constant mean and amplitude sinusoidal loading for a certain number of cycles (typically below 20,000). This loading block is repeated in a series of analogous blocks, increasing the load amplitude while maintaining a constant mean value or a constant load ratio. The temperature measured during each loading block is processed to obtain specific thermal metrics that are then plotted against the loading amplitude of each block. The intrinsic dissipation of the material is then correlated with the trend of such thermal metrics. It is usually found that beyond a certain stress amplitude, the observed thermal metric starts experiencing a significant variation, most often in the form of a higher increase-rate, which is considered as a signature of the onset of dissipative irreversible damage mechanism and accumulation eventually bringing the material to develop macroscopic cracking and fatigue failure.

Since the original works of Luong et al. [8] and La Rosa and Risitano [9], the *fatigue thermographic method* has continuously expanded, with the proposition of different thermal, energetic and entropic metrics, as well as procedures to enhance and elaborate signatures of intrinsic dissipation. Among the most commonly employed methods, many rely on evaluating temperature and its slow evolution over time. This exposes the metrics analyzed to spurious environmental influences, such as environmental energy reflection and heat conduction/convection towards the sample surroundings [1, 29, 30]. Alternative temperature metrics, intrinsically more robust against environmental influences, are those derived from the harmonic content of the temperature signal, and hence used in the so-called Harmonic Methods [7]. Such harmonic temperature metrics are primarily correlated to reversible thermomechanical heat sources and are modulated at frequencies higher than the usual environmental fluctuations, making them more insensitive to spurious variations. In an ideally linear elastic loading regime, the main reversible thermomechanical coupling is the thermoelastic effect [31]. Thermoelastic stress analysis (TSA) is an experimental technique based on lock-in correlation to extract the thermoelastic harmonic from the temperature signal [32]. In its simplest form, the temperature variation ΔT induced by the thermoelastic effect in an isotropic material subject to sinusoidal loading can be expressed as

$$\Delta T(t) = -\frac{\alpha}{\rho c_p} T_o \Delta I_1 \sin\left(2\pi f_L t + \phi\right) \tag{1}$$

where ΔI_1 represents the amplitude of the first stress invariant variation, ρ is the density, C_p the specific heat at constant pressure, α the coefficient of thermal expansion (CTE), T_o the absolute mean temperature, f_L the loading frequency and ϕ the phase shift between the loading wave and the thermoelastic wave. Under adiabatic conditions, ϕ is zero or 180°, depending on the stress-invariant fluctuation with respect to the applied load. Equation (1) shows that the amplitude of the temperature harmonic at the frequency f_L is linearly correlated to the amplitude of the first stress-invariant modulation.

A more general characterization of the temperature change with time would include also a second harmonic term $2f_L$, so that Equation (1) can be rewritten as

$$\Delta T(t) = A_\omega \sin\left(\omega t + \phi_\omega\right) + A_{2\omega} \sin\left(2\omega t + \phi_{2\omega}\right) \tag{2}$$

where $\omega = 2\pi f_L$ is the angular load frequency.

Harmonic methods are based on adopting the harmonic metrics $A_\omega, A_{2\omega}, \phi_\omega$ and $\phi_{2\omega}$ in the stepwise procedure, plotting them versus the stress amplitude of each loading block, to identify signatures of the onset of intrinsic inelastic dissipation. This also offers the advantage of significantly expediting the analysis process, as the harmonic content is typically derived within a few seconds of high-frequency temperature sampling and then processed using appropriate frequency domain analysis algorithms, such as *Discrete Fourier Transform* or *Least Square Fitting*. The ability of the four harmonic metrics to identify intrinsic dissipation has been recently reviewed in [27]. The term A_ω is mainly dominated by the thermoelastic signal which is supposed to remain linearly correlated to the stress amplitude as long as the material is linear elastic. However, several works report a slight sensitivity of A_ω to intrinsic dissipation [10, 12, 16, 19]. Some explanations for such observations include the increase of the mean temperature T_o (which composes the thermoelastic signal, as shown in (1)) [27], or the influence of material inelastic changes on the thermoelastic constant [33]. The correlation of ϕ_ω with intrinsic dissipation is proposed and discussed in [14, 20]. The amplitude of the second harmonic $A_{2\omega}$ is arguably the most effective harmonic metric to monitor intrinsic dissipation. Enke [34] already observed that energy dissipation increases at peaks and troughs of the loading wave, thus producing a 2ω modulation on the temperature signal. Some theoretical confirmations of Enke's explanation have recently been provided [20, 25, 35, 36]. The use of $A_{2\omega}$ as a dissipation index during fatigue loading was introduced by Bremond et al. [37] and Krapez [10], who also used this metric in a step-wise FLTM test on a stainless steel 316 L and an aluminum alloy 7010. Since then, several other works have reported the adoption of $A_{2\omega}$[11, 12, 14-20, 35, 36, 38-40].

More recently, some authors have proposed the phase of the second harmonic, $\phi_{2\omega}$, as a potential additional metric to

monitor the evolution of dissipation [15, 27, 28, 41]. As mentioned above, the dissipative second harmonic wave has its peaks positioned near the peaks and troughs of the first thermoelastic harmonic. At small loading amplitudes, when conditions for intrinsic dissipation are not yet fully established, the $\phi_{2\omega}$ is expected to have a different relative position compared to the first thermoelastic harmonic. The work from [15] has suggested that this position is dictated by spurious second harmonic components of the imposed loading wave. It is reported that the loading signal from testing machines is not a pure sinusoidal wave and a spurious second harmonic is usually introduced, which produces a thermoelastic signal at $\phi_{2\omega}$, hereinafter indicated as Second Loading Harmonic (SLH) to distinguish it from the Second Dissipative Harmonic (SDH). On the other hand, [27] observed that the higher order Thermoelastic Law, as developed in [42], predicts the existence of a Second Thermoelastic Harmonic (STH), that under uniaxial stresses is opposite in phase to the SDH when the derivative of Young's modulus with respect to temperature is negative; that is, $dE/dT < 0$. Therefore, the second harmonic, evaluated through a TSA experiment, will be the result of the combination of three components:

- A dissipative component that should emerge as dominant beyond a certain load amplitude threshold, with peaks closely aligned to the peaks and troughs of the first harmonic thermoelastic wave;
- A thermoelastic component that is the response to a second harmonic load-component introduced by mechanical vibrations [15, 28] or imperfect load application by the testing machine, and whose phase is generally unknown;
- A thermoelastic component predicted by the higher order thermoelastic effect, dependent on the thermomechanical properties of the analyzed material (in particular $\frac{\partial E}{\partial T}$), with a well established phase.

The above terms can also be made explicit in (2), which can be rewritten as

$$\begin{aligned}\Delta T(t) &= A_{\omega}\sin(\omega t+\phi_{\omega}) - A_{2\omega D}\cos(2\omega t)\\ &+ A_{2\omega L}\sin(2\omega t+\phi_{2\omega L}) + A_{2\omega T}\cos(2\omega t)\end{aligned} \tag{3}$$

where the STH and SDH waves have well-defined phase positions related to the sin loading wave, as reported in [27], while the SLH has a not predictable phase shift indicated by $\phi_{2\omega L}$.

The progression of the second harmonic wave is expected to present two main stages. Initially, at lower stress amplitudes, the phase $\phi_{2\omega}$ is expected to arise from the interplay of the two competing terms, STH and SLH, both associated with the thermoelastic effect. With an increase in the loading amplitude, a second stage will predominate, during which the $\phi_{2\omega}$ is mainly governed by the SDH. It can be observed that the coexistence of thermoelastic second harmonic waves with the dissipative wave might badly condition the accuracy of the second harmonic amplitude $A_{2\omega}$ in detecting the onset of dissipation, if not properly decoupled of the thermoelastic terms. On the contrary, monitoring the evolution of the second harmonic phase might better reveal the mutual influence of thermoelastic and dissipative waves as the loading amplitude increases. Indeed, the use of the Second Harmonic amplitude as a successful metric for the FLTM is mainly documented for steels, where the second-order thermoelastic effects are more negligible [42], and a significant intrinsic dissipation is generally observed. Krapez et al. [10] conducted one of the very few studies evaluating the second harmonic in an aluminum alloy sample during a stepwise test. They report a gradual increase of the second harmonic of temperature, and it remains unclear whether the deviation from linearity observed in the study is a result of dissipation development or a second-order thermoelastic effect. This uncertainty highlights the importance of gaining a more comprehensive understanding of these parameters by combining both amplitude and phase information.

In light of the above, the present work investigates means of decoupling the influence of various concurrent second harmonic terms under nominally sinusoidal tensile loading. A specific signal post-processing framework has been developed to decouple the three second harmonic contributions. The key and novel aspects of the proposed approach are:

- The analysis of the harmonic components of the applied load to both identify components at twice the loading frequency, and quantify the influence of spurious load components.
- The evaluation of the higher order thermoelastic effect and the subsequent correction of its influence with respect to the second harmonic metrics.

The final aim of the study is to evaluate if decoupled dissipative second harmonic amplitude and phase metrics can improve the detection of intrinsic dissipation in metals known for their mild thermo-mechanical coupling. For this purpose, the proposed procedure is applied to Al 2024 T3 tensile specimens: renown for their poor dissipative behavior [43] and characterized by a high thermal diffusivity, which makes the detection of intrinsic dissipation particularly challenging.

2 | Materials and Methods

2.1 | Experiments

The material investigated in this study is the aluminum alloy AL 2024 T3, with dog-bone-shaped samples cut from a plate and subject to traction-compression tensile sinusoidal loading. The choice of this material was based on its tendency to exhibit a pronounced variation of Young's modulus with temperature [42, 44], and hence a strong second-order thermoelastic effect [42].

The geometry of the specimen was defined in accordance to the sub-size specimen described in the ASTM standard E8 [45], with a nominal cross sectional area of $A = 3 \times 6$ mm^2. The surface of each specimen was cleaned with acetone and then painted with matt black paint to uniform and increase infrared emissivity.

A FLIR X6540sc cooled sensor thermal camera was used to measure the temperature of the surface of the specimen. The integration time was set equal to 659 μ s while the sampling frequency

was selected to 200 Hz. An analog output signal from the load cell is connected to the lock-in input of the thermal camera to acquire the loading signal synchronously to the thermograms.

A sinusoidal load was applied employing an Instron ElectroPuls E10000 electro-dynamic testing machine, with a loading frequency of 15 Hz and load ratio $R = -1$ ($R = \frac{\sigma_{min}}{\sigma_{max}}$). Tests have been conducted following a step-wise approach, where blocks of increasing loading amplitude have been applied to the specimens. Each loading step had a duration of 300 s, with the thermal camera acquiring the last 30 s of each block, after ensuring the stabilization of the surface temperature.

The choice of a 15-Hz loading frequency is sufficiently high to ensure adiabatic conditions [1] and allows for the detection of intrinsic dissipative heat generation. This frequency has proven effective in capturing early-stage dissipation phenomena even in aluminum alloys, as demonstrated in [2].

Table 1 reports all the details of the experimental testing parameters.

2.2 | The Higher Order Thermoelastic Theory

The heat diffusion equation provides a comprehensive description of the local thermodynamic state and the thermomechanical heat sources for a specific point within a solid body [27, 46, 47]. Among the various terms describing the thermo-mechanical couplings, this study considers conditions where two terms prevail: (i) the thermoelastic heat source and (ii) the dissipative heat source. The prediction of temperature changes associated with the thermoelastic and dissipative heat sources under sinusoidal loading follows the same development outlined in [27]. In particular, it is initially assumed that the material behaves as linear elastic under low-mean and low-amplitude cyclic strain (as expected under high cycle fatigue), and the loading frequency is high enough to allow thermoelastic-effect induced temperature changes under adiabatic conditions. In this scenario, the thermoelastic heat source is the main thermomechanical coupling in the heat diffusion equation, which can be rewritten as [48]

$$\rho C_\epsilon \frac{\dot{T}}{T} = \frac{\partial \sigma_{ij}}{\partial T}\dot{\epsilon}^e_{ij} \tag{4}$$

where dotted terms denote time derivatives, ρ and C_ϵ the material density and specific heat at constant volume, and σ_{ij} and ϵ^e_{ij} the stress and elastic strain tensors. The derivative of the stress tensor to temperature can be further developed considering the generalized Hooke's elastic law. In [42], this was performed considering the temperature dependence of the elastic parameters. The resulting expression as a function of stresses is reported:

$$\begin{aligned}\rho C_\epsilon \frac{\dot{T}}{T} &= -\left[\alpha + \left(\frac{\nu}{E^2}\frac{\partial E}{\partial T} - \frac{1}{E}\frac{\partial \nu}{\partial T}\right)\sigma_{kk}\right]\dot{\sigma}_{kk} \\ &+ \left(\frac{1+\nu}{E^2}\frac{\partial E}{\partial T} - \frac{1}{E}\frac{\partial \nu}{\partial T}\right)\sigma_i\dot{\sigma}_i\end{aligned} \tag{5}$$

where α the coefficient of thermal expansion, σ_{kk} the first stress invariant and σ_i a principal stress ($i = 1,2,3$). In the case of a uniaxial stress field, (5) can be simplified in

$$\rho C_\epsilon \frac{\dot{T}}{T} = -\left[\alpha - \frac{1}{E^2}\frac{\partial E}{\partial T}\sigma\right]\dot{\sigma} \tag{6}$$

Integrating Equation (6) over time requires a time variation law of the stress component, that is here expressed as a sine wave: $\sigma = \sigma_m + \sigma_a \sin(\omega t)$ and $\dot{\sigma} = \sigma_a \omega \cos(\omega t)$. Integrating between an initial instant $t = 0$ ($T = T_o,\ \sigma = \sigma_m$) and a final time t yields

$$\begin{aligned}\rho C_\epsilon \log\left[\frac{T}{T_o}\right]_0^t &= -\left[\alpha - \frac{1}{E^2}\frac{\partial E}{\partial T}\sigma_m\right]\sigma_a\omega\left[\frac{\sin(\omega t)}{\omega}\right]_0^t \\ &+ \left[\frac{1}{E^2}\frac{\partial E}{\partial T}\frac{{\sigma_a}^2\omega}{2}\right]\left[-\frac{\cos(2\omega t)}{2\omega}\right]_0^t\end{aligned} \tag{7}$$

If the temperature change is small compared to the average value T_o, then the log term reduces to $\Delta T/T_o$, and the relationship Equation (7) becomes:

$$\begin{aligned}\rho C_\epsilon \frac{\Delta T}{T_o} &= -\left[\alpha - \frac{1}{E^2}\frac{\partial E}{\partial T}\sigma_m\right]\sigma_a \sin(\omega t) \\ &+ \left[\frac{1}{E^2}\frac{\partial E}{\partial T}\frac{{\sigma_a}^2}{4}\right]\left(1 - \cos(2\omega t)\right)\end{aligned} \tag{8}$$

Retaining the time varying terms in Equation (8), it is seen that these comprise two harmonics: $\sin(\omega t)$ and $-\cos(2\omega t)$, which have a well-established relative phase shift. Equation (8) can also be written as

$$\rho C_\epsilon \frac{\Delta T}{T_o} = -\left[\alpha - \frac{1}{E^2}\frac{\partial E}{\partial T}\sigma_m\right]\sigma_a \sin(\omega t) + \left[\frac{1}{E^2}\frac{\partial E}{\partial T}\frac{{\sigma_a}^2}{2}\right]\sin^2(\omega t) \tag{9}$$

which clearly shows that the $sin^2(\omega t)$ term has a 2ω modulation whose peaks align with the peaks and troughs of the $sin(\omega t)$ term when both coefficients have the same sign.

In light of the above, the temperature variation ΔT from a tensile test can be expressed as [42]

$$\Delta T = -T_o(K_o - K_1\sigma_m)\sigma_a \sin(\omega t) - T_o K_2(\sigma_a)^2 \cos(2\omega t) \tag{10}$$

where T_o denotes the average temperature in the sample and σ_m and σ_a represent the mean and amplitude of the applied stress, respectively; K_o, K_1, and K_2 are the thermoelastic constants that can be defined as

$$K_o = \frac{\alpha}{\rho C_\epsilon};\ K_1 = \frac{1}{\rho C_\epsilon}\frac{1}{E^2}\frac{\partial E}{\partial T};\ K_2 = \frac{K_1}{4} \tag{11}$$

TABLE 1 | Testing parameters for $R = -1$.

Loading ratio	$R = -1$
Tested specimens	AL3 AL4 AL5 AL6
Stress amplitude	60, 80, 100, 120, 130, 140, 150, 160, 180, 200 MPa
Loading frequency	15 Hz
Sampling frequency	200 Hz
Time window	30 s (450 loading cycles)

In addition to the well-known first-order thermoelastic signal, which is modulated at the same frequency as the applied load, it is essential to highlight the presence of the second-order thermoelastic effect as indicated by Equation (10). This effect leads to a reversible temperature variation occurring at twice the loading frequency and modulated by a cosine wave.

Table 2 reports a representative value of $\frac{\partial E}{\partial T}$ for the aluminum alloy investigated in this study, alongside values reported in the literature for other metallic alloys that have been employed in TSA studies involving the higher-order formulation. In most cases, $\frac{\partial E}{\partial T}$ is negative, resulting in $K_2 < 0$ and a second harmonic thermoelastic contribution modulated as $\cos(2\omega t)$, according to Equation (10). An exception to this behavior is observed in shape memory alloys, such as Nitinol, for which a positive $\frac{\partial E}{\partial T}$ yields a second-harmonic thermoelastic response modulated as $-\cos(2\omega t)$ [48].

The other element to consider is the activation of a dissipative heat source upon reaching a specific stress level, which involves the accumulation of inelastic strain over each loading cycle [25, 26, 34, 46]. In the case of a reversed loading test ($R = -1$), dissipative heat is generated at each peak and trough of the loading cycle. This irreversible heat generation, followed by subsequent cooling, produces a thermographic signal rich in harmonic content [25]. When analyzed in the frequency domain, this signal reveals a pronounced second harmonic component, ($\Delta T_{d2\omega}$) modulated at twice the loading frequency, that can be expressed as

$$\Delta T_{d2\omega} = -T_d \cos(2\omega t) \tag{12}$$

As illustrated by Equation (12), the second harmonic of dissipation is modulated as $-\cos(2\omega t)$. Consequently, the resulting temperature variation caused by the activation of this heat source will be in opposite phase compared to the Second Thermoelastic Harmonic component described in Equation (10).

2.3 | Harmonic Analysis of the Load Signal

Although the imposed load should ideally be a purely sinusoidal wave with a single harmonic component, some studies have observed the presence of higher loading harmonics. These can be introduced by intrinsic inaccuracies of the testing machine controller, but could also originate from mechanical vibrations of the heavy mechanical grips and the frame of the testing machine [15, 27, 28]. The presence of these harmonics could also depend on the material, the applied load range and frequency, and the tuning of the testing machine. Both the analog load and a reference signal extracted directly from the acquired thermograms, exploiting the so-called "edge effects" described in [50], are analyzed. In the present work, such an edge effect is generated by focusing the Region Of Interest (ROI) on the edge of the alignment device attached to the moving grip (hereinafter referred to as ROI1), as shown in Figure 1. The signal averaged within the ROI1 (see Figure 1a,b) is composed by a hot portion belonging to the alignment device and a cold portion corresponding to the background. Therefore, the movement of the alignment grip produces a modulated wave which describes the deformation applied to the sample.

Figure 1c reports the Discrete Fourier Transform (DFT) spectrum of the ROI1 and when a stress amplitude of 180 MPa was applied. The Fourier analysis of the averaged ROI1 signal provides a broad overview of the load frequency content. In addition to the main applied load component at 15 Hz, other peaks at its integer multiples (i.e., 30 and 45 Hz) are found. The presence of such a significant spurious Second Loading Harmonic introduces an undesired first-order thermoelastic effect that combines with the previously described components. This load-related second harmonic then overlaps with the previously described Second Thermoelastic and Dissipative Harmonic terms. A similar harmonic content is found in the temperature variation, as shown in the Fourier spectrum of the ROI2, positioned in the central part of the specimen.

Finally, the analysis of an additional ROI comprising only the background allows to assess the noise present in the acquisition: a spurious component at about 30 Hz is found in all ROIs, to be attributed to vibrations of the thermal camera [27].

The analysis of the load signal is repeated for each thermal acquisition, to quantify the harmonic components of the applied load at different frequencies. Unlike the other second harmonic components discussed earlier, which exhibit specific phase shifts attributable to their physical mechanisms, the phase of this load component is expected to be random. Therefore, an individual evaluation of such components is needed for each load step.

In the signal processing framework proposed in the present work both reference signals are employed: The amplitude of the first and second loading harmonics are obtained from the analog lock-in signal fed into the thermal camera, while the edge effect signal (ROI1 in Figure 1) is employed to check and account for potential undesired phase delays between the analog reference and the sampled thermograms.

TABLE 2 | $\frac{\partial E}{\partial T}$ for metals commonly used in TSA applications.

Material	$\frac{\partial E}{\partial T}\left[\frac{MPa}{K}\right]$	Reference
Aluminum	−36	[42]
Stainless steel	−19	[49]
Titanium	−48	[42]
Nitinol, austenite	2230.6	[49]
Nitinol, martensite	49.5	[49]

2.4 | Modelled Harmonic Content

Assuming that the main component of the load follows a purely sinusoidal wave, the resultant stress will induce a first-order thermoelastic effect. The modelled second harmonic response reveals the following:

- The second harmonic arising form the second-order thermoelastic theory is characterized by an expected phase modulation of a cosine wave, that is, a $cos(2\omega)$.

- A first-order thermoelastic signal arises from the presence of a spurious load second harmonic component with initial random amplitude and phase.
- The dissipative second harmonic, that is expected to arise after a certain load threshold has been reached, exhibits a specific modulation of a negative cosine wave, that is, $-cos(2\omega)$.

The relative phase shifts described are summarized in Table 3.

2.5 | Harmonic Components Filtering

In this work, the signal sampled from the IR camera was processed using the least-squares fitting (LSF) procedure [51]. In the context of TSA signal processing, this methodology is generally preferred since it allows for the comprehensive characterization of the harmonic component (evaluation of amplitude and phase), without concerns about spectral leakage or frame drop correction, the only requirement being an accurate selection of the loading frequency to be filtered [51].

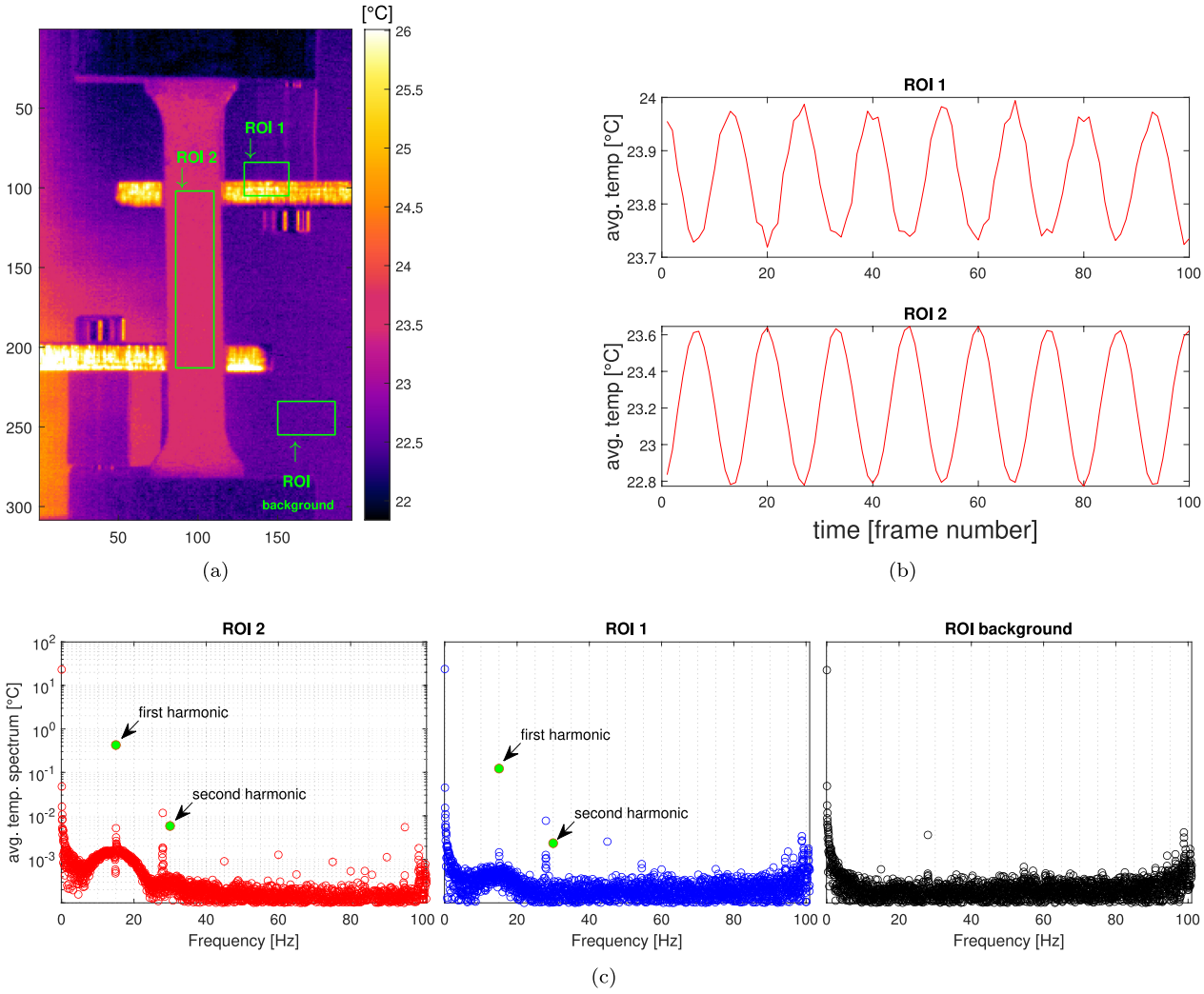

FIGURE 1 | (a) ROIs selected for the analysis: load signal (ROI 1), sample temperature signal (ROI 2), and background signal; (b) average temperature plots from ROI 1 and ROI 2; (c) harmonic content of the average ROIs temperatures. [Colour figure can be viewed at wileyonlinelibrary.com]

TABLE 3 | Relative phase positions of load, thermoelastics, and dissipative terms.

Signal component	Time modulation	Phase shift with reference to a pure sine wave	Reference equation
Load	$\sin(\omega t)$	0°	
First harmonic	$-\sin(\omega t)$	± 180°	Equation (1)
Second-order second harmonic	$\cos(2\omega t)$	90°	Equation (10)
Dissipation second harmonic	$-\cos(2\omega t)$	−90°	Equation (12)
Load second harmonic	$\cos(2\omega t + ?)$	Unknown	

The LSF approach employed here involves fitting each point within the field of view (FoV) of the thermal camera by means of the following equation:

$$T(t) = T_o + B \cdot t + E\cos(\omega \cdot t - \Phi_E) + D\cos(2\omega \cdot t - \Phi_D) \quad (13)$$

where t is time; T_o is the absolute temperature of the sample; B represents a linear increase of the temperature; ω is the angular frequency of the applied sinusoidal load; E is the amplitude of the first harmonic of temperature (i.e., the thermoelastic signal); Φ_E is the phase of the first harmonic, expected to be opposite to the applied load (i.e., $\Phi_E = \pi$); D is the second harmonic amplitude, resultant of all the components discussed earlier; lastly, Φ_D is the phase of the second harmonic and should give insights on the underlying physical mechanisms dominating the second harmonic parameter.

2.6 | Proposed Methodology for Data Correction

In this section, a simple framework is proposed for the evaluation of the dissipative component of the temperature signal. It is worth pointing out that the proposed correction will affect only the second harmonic, and not the first harmonic, which will remain unchanged.

The correcting procedure consists of the following steps:

1. Lock in of the temperature signal in the central area of the specimen (ROI 2 of Figure 1a) and evaluation of the first-harmonic amplitude E with Equation (13).
2. Selection of an appropriate ROI for the evaluation of the reference signal (i.e., ROI 1 in Figure 1a) and application of the LSF to the load signal from the testing machine to evaluate its amplitudes in the first and second harmonics (L_1 and L_2) and phases (Φ_{L_1} and Φ_{L_2}). The signal from ROI 1 is used to check for the presence of any phase delays between the thermograms and the analog reference loading signal fed into the thermal camera lock-in input.
3. Calculation of the first-order thermoelastic effect due to the load second harmonic [27]:

$$E_{L_2} = \frac{L_2}{L_1}E \quad (14)$$

and reconstruction of the wave in the time domain as

$$\Delta T_{2\omega L} = E_{L_2}\cos(2\omega t - \Phi_{L_2} + \pi) \quad (15)$$

The 180° phase shift is introduced to transform the load modulation into the corresponding thermoelastic effect. Information about the amplitude and phase of the second harmonic of the load are obtained from step 2.

4. Evaluation of the second order, second harmonic thermoelastic effect, as described in Equation (10). In this work, a refererence $\partial E/\partial T$ has been taken from [42], and experimentally confirmed as described in Section 3.4.
5. Subtraction of the signal obtained from steps 3 and 4 to the measured temperature signal from the points of ROI2. The subtraction has to be performed in the time domain, to correctly account for the phase shift induced by the different second harmonic influencing components. Also, all signals are reported into a common phase reference, following the procedure outlined in [27]. This operation is feasible since the phase shift of the load Φ_{L_1} is known from step 2.
6. Application of the LSF filtering to the corrected frames and analysis of the second harmonic metrics.

3 | Results and Discussion

This section presents and discusses the results obtained before and after applying the proposed correction methodology.

The results are presented as averages of the full-field measurements for the four specimens tested to provide a comprehensive analysis. This approach has been shown to be valid for identifying dissipation in similar tests [27]. Additionally, dispersion bars are included for each stress level to indicate the standard deviation among the analyzed specimens.

3.1 | Mean Temperature and First Harmonic Metrics

Figure 2 illustrates the evolution of the mean temperature and the first harmonic amplitude.

The mean temperature increase shown in Figure 2a exhibits a really modest rise, limited to around 1° between the first and last test. Despite the high loading frequency employed, the negligible increase in temperature might mostly be attributed to the high thermal diffusivity of the aluminum. However, this parameter starts to slightly deviate from the linear behavior at a stress level of about 140 MPa.

The first harmonic amplitude exhibits a fairly linear behavior over the whole range of step amplitudes, showing no clear evidence of a deviation due to dissipation or a change of trend across the expected fatigue limit (which for this AL alloy is expected at around 138 MPa [52]). Figure 2b clearly shows that, for none of the applied stresses, the variation of the thermoelastic first harmonic E significantly deviates from the expected linear behavior. According to Equation (1), the modest rise in the mean temperature in the ROI does not promote nonlinear variations in the first harmonic. The observed behavior is also in agreement with some recent observations from [25], which show that dissipative components may arise also at the first harmonic frequency only when the applied stress ratio is $R > 0$.

3.2 | Analysis of the Second Harmonic Metrics

Figure 3 presents the plots of the second harmonic amplitude (a) and phase (b) prior to implementing the correction procedure outlined in Section 2.6.

Figure 3a clearly shows that the second harmonic amplitude deviates from the linear fit only at the highest applied

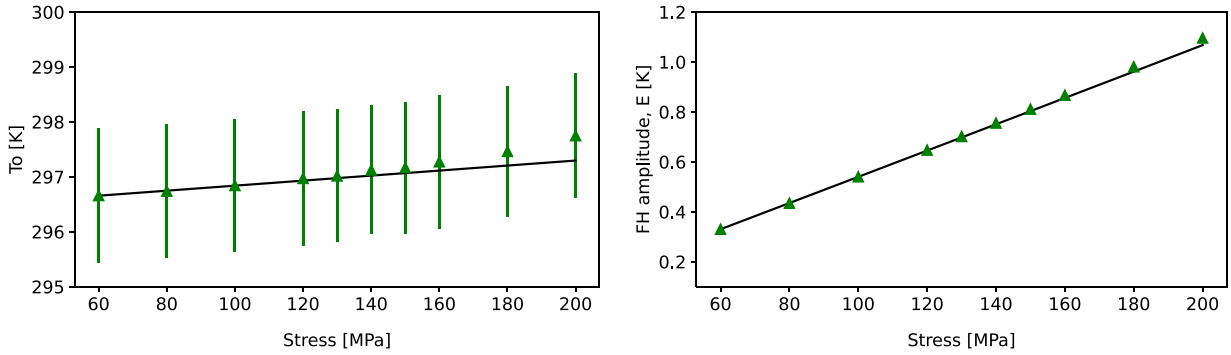

FIGURE 2 | (a) Mean temperature T_o and (b) first harmonic amplitude E. [Colour figure can be viewed at wileyonlinelibrary.com]

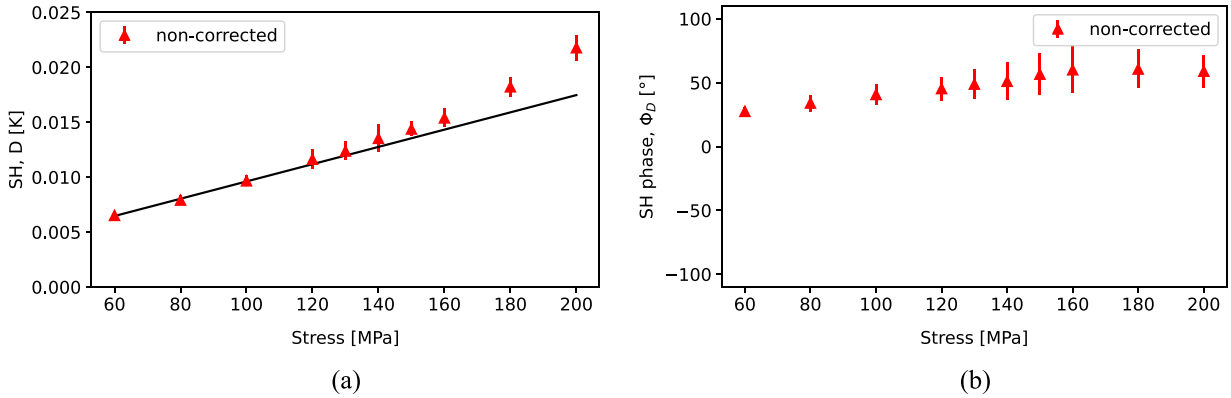

FIGURE 3 | (a) Second harmonic amplitude D and (b) second harmonic phase Φ_D. Plots obtained before the application of the proposed correction. [Colour figure can be viewed at wileyonlinelibrary.com]

stresses. This behavior could be attributed to the inherent 180° phase shift between the two dominant physical phenomena—namely, the second-order thermoelastic effect and dissipation—which leads to destructive interference between the temperature changes modulated at the second harmonic, delaying the rise of the second harmonic parameter. However, the second harmonic phase in Figure 3b exhibits a smooth transition to a value of approximately 60°, that suggests that the prevailing physical phenomenon driving the second harmonic is the second order thermoelastic effect (modulated at +90°, Table 3).

The distinct behavior of the second harmonic phase can be observed by examining the histograms presented in Figure 4 for specimen AL6. Figure 4 displays four histograms (right), alongside their respective full-field maps (left), for stress levels of 60, 120, 140, and 200 MPa. The histograms clearly depict the presence of a higher peak around +90°, related to the second-order thermoelastic effect, and a smaller contribution around −90°, which could be linked to dissipation. The peak corresponding to the second-order thermoelastic effect is present across all stress levels. This is also noticeable in the full-field maps, where the bimodal trend is particularly visible at lower load levels, with a nearly uni-modal behavior aligned to the second-order thermoelastic effect at higher loading values. It is important to note that the second-order thermoelastic effect is proportional to the square of the applied stress amplitude, as described by Equation (10), and its influence strongly increases with the loading amplitude, thus acting as a competing mechanism against the Dissipation Second Harmonic and affecting the ability of D to pinpoint the onset of dissipation.

3.3 | Analysis of the Second Harmonic Component of the Load Signal

For each performed test, as outlined in Section 2.6, the load signal from the load cell was extracted and its harmonic content analyzed.

Figure 5 presents the second harmonic amplitude and phase for the four specimens. The amplitude is expressed as the ratio between the second and first harmonics of the load ($\frac{L_2}{L_1}$), and the phase is expressed by shifting the load signal to a common reference (the first harmonic of the load as a pure sine wave).

Interestingly, all analyzed curves obtained from different specimens exhibit a similar trend in terms of both amplitude and phase. The amplitude of the second harmonic of the load is typically lower than 0.5% of the first harmonic, and the phase values display a decreasing trend with increasing load. This consistent behavior might either be an intrinsic characteristic of the testing machine or a response of the load cell to changes in the material's behavior under increased load.

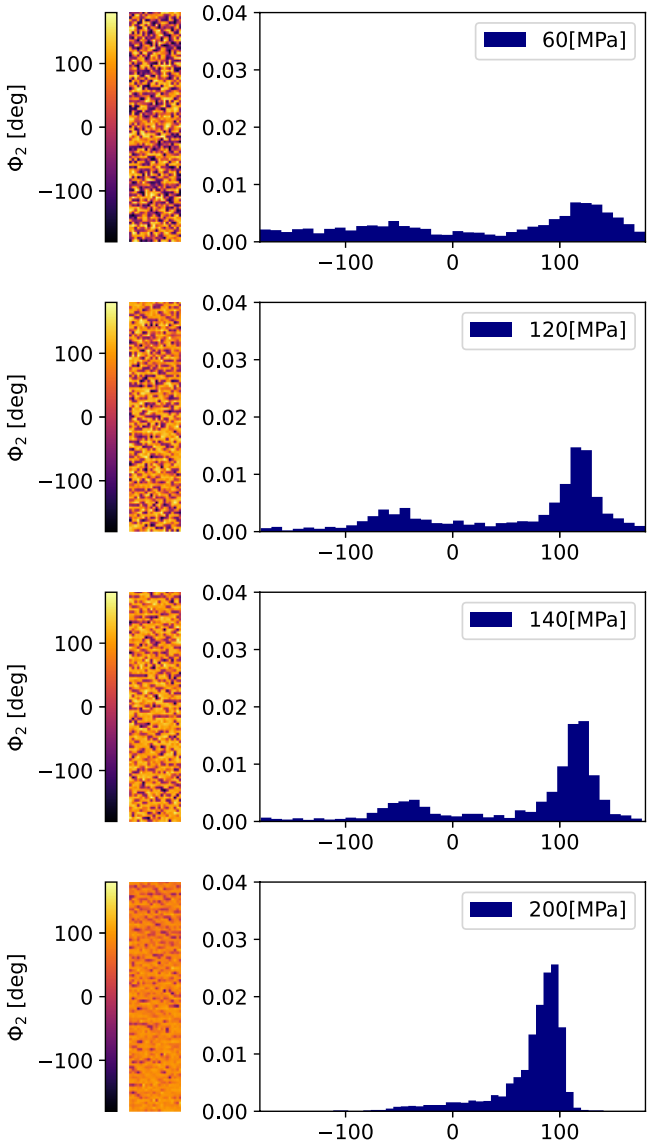

FIGURE 4 | (Left) full field maps and (right) histogram of the distribution of the second harmonic phase Φ_D. Data obtained before the application of the proposed correction procedure. [Colour figure can be viewed at wileyonlinelibrary.com]

If the latter hypothesis is correct, the second harmonic of the load signal could provide valuable information about the onset of dissipative behavior in the material during stepwise loading. Figure 6 shows the first-order thermoelastic effect derived from the second harmonic of the load, applying Equation (14). Surprisingly, this curve reveals a bilinear trend, with a distinct increase in the thermoelastic effect beginning at 130 MPa.

3.4 | Procedure for the Evaluation of the Thermoelastic Constant K_2

The correction procedure outlined in Section 2.6 requires the determination of the second-order thermoelastic effect. To avoid relying on theoretical thermomechanical properties of the material, the higher-order thermoelastic constant K_2 is determined directly from the measured second harmonic of temperature. The analysis of Φ_D in Figure 3b showed that the dominant thermomechanical component in the second harmonic of temperature is the second-order thermoelastic effect.

The determination of the thermoelastic constant K_2 is performed by fitting a second-order polynomial to the second harmonic of temperature. In a scenario where the only effect is the second-order thermoelastic effect, Equation (10) can be written as:

$$\frac{\Delta T}{T_o} = -K_2\sigma_a^2 \tag{16}$$

where $\frac{\Delta T}{T_o}$ is measured and σ_a^2 is known, since the tests are performed in load control.

To reduce the influence of noise and achieve a more accurate determination of K_2, the fitting of Equation (16) is performed on the average temperature signal; that is, the signal inside the ROI is averaged before applying the lock-in algorithm. Additionally, the thermoelastic effect generated by the second harmonic of the load, identified in the previous section, is accounted for and subtracted (see Section 2.6, step 3). The temperature second harmonic amplitude and phase, after correcting for the load's second harmonic, are presented in Figure 7.

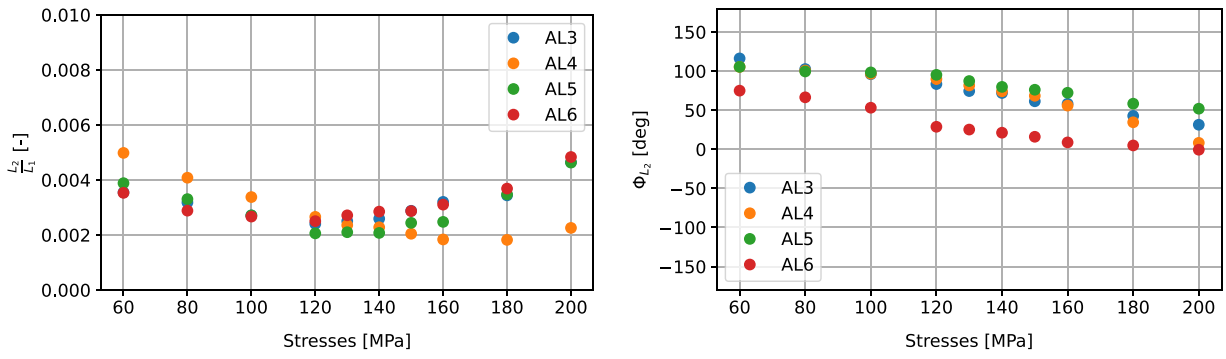

FIGURE 5 | (a) Ratio between the second and first harmonics of the load signal. (b) Phase of the second harmonic component of the load Φ_{L_2}. Results are reported for each test. [Colour figure can be viewed at wileyonlinelibrary.com]

All experimental points are included in the fitting procedure, since their phase values are reasonably close to the theoretical +90°. The results of the fitting procedure are shown in Figure 7a. The green fitting line closely approximates the second harmonic of temperature, and the calculated value of the thermoelastic constant is $K_2 = 7.14 \times 10^{-10} \frac{1}{\mathrm{MPa}^2}$. Inputting $\rho = 2780 \frac{\mathrm{Kg}}{\mathrm{m}^3}$, $C_p = 875 \frac{\mathrm{J}}{\mathrm{KgK}}$ and $E = 73000\,\mathrm{MPa}$ [52], in the definition of K_2 (Equation 11), a value of $\frac{\partial E}{\partial T} = -37.1 \frac{\mathrm{MPa}}{\mathrm{K}}$ is found, in excellent agreement with $\frac{\partial E}{\partial T} = -36 \frac{\mathrm{MPa}}{\mathrm{K}}$ reported in [42].

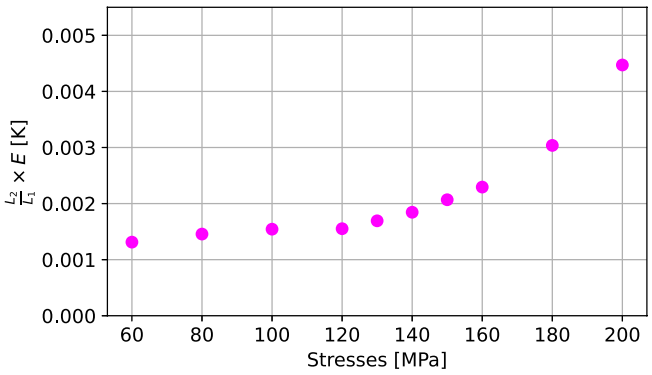

FIGURE 6 | First-order thermoelastic effect of the second harmonic, obtained multiplying the average of all curves in Figure 5a by E. [Colour figure can be viewed at wileyonlinelibrary.com]

3.5 | Application of the Proposed Methodology

Figure 8 displays the plots of the second harmonic amplitude (a) and phase (b) after implementing the correction procedure outlined in Section 2.6.

The corrected plots of the second harmonic amplitude and phase permit several noteworthy observations. In Figure 8a, the amplitude of the second harmonic clearly detects a deviation from the linear behavior observed at lower stress levels. However, instead of presenting a distinct increase, the bi-linear trend appears as a pseudo-convergence, starting at a stress value of around 130 MPa.

The second harmonic phase in Figure 8b remains very close to zero for all the analyzed stress levels. This indicates no transition to a dissipative behavior, suggesting that no clear signature of dissipation can be identified in the averaged phase results.

The average phase close to zero can be explained by examining Figure 9 (right), which presents the histograms of the same specimen and the same four stress levels previously shown in Figure 4 (right). After the correction, the histograms display the expected bi-modal trend for all stress levels, but no clear transition to either the dissipative or higher order thermoelastic behavior is observed.

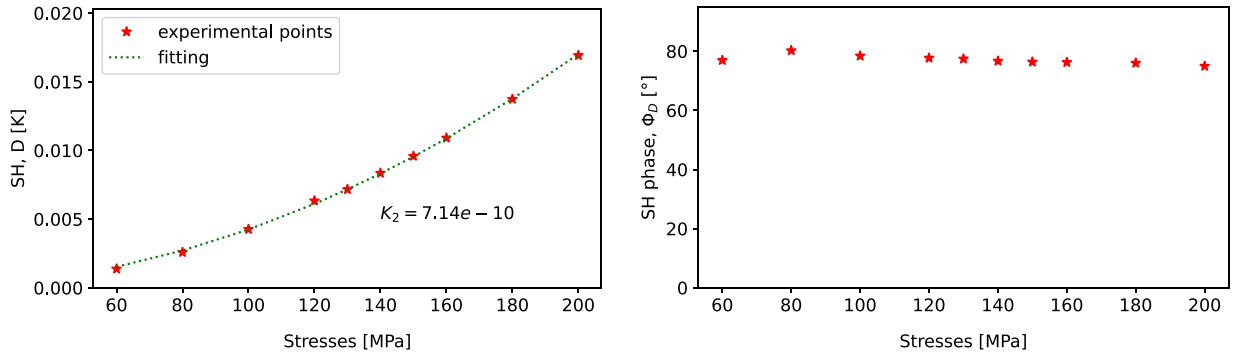

FIGURE 7 | (a) Second harmonic amplitude D, with the experimentally obtained K_2 thermoelastic constant. (b) Second harmonic phase Φ_D. Plots obtained after subtracting the load's second harmonic component. [Colour figure can be viewed at wileyonlinelibrary.com]

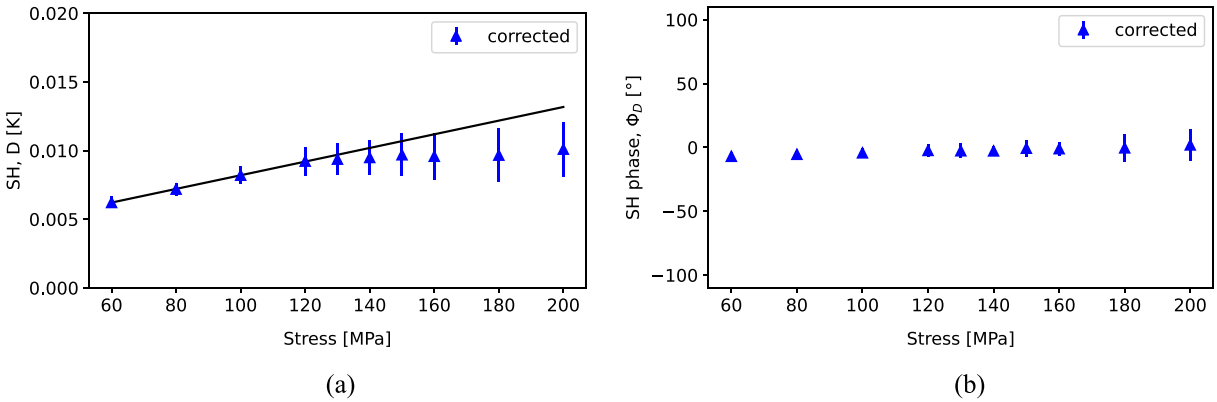

FIGURE 8 | (a) Second harmonic amplitude D, (b) Second harmonic phase Φ_D. Plots obtained after applying the correction. [Colour figure can be viewed at wileyonlinelibrary.com]

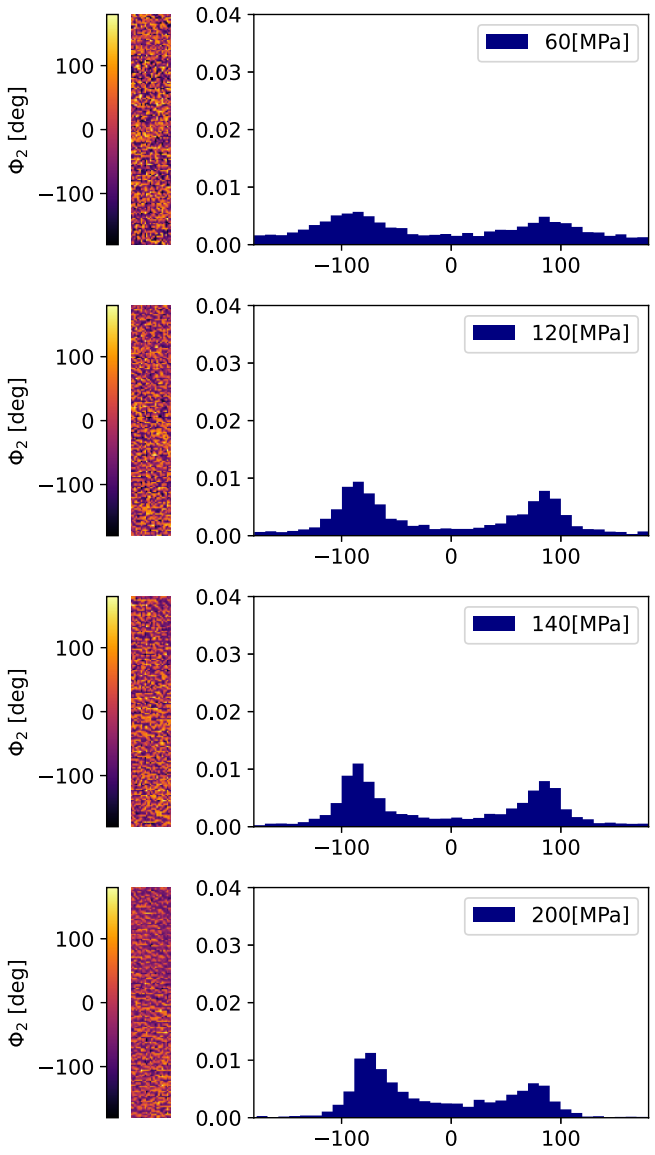

FIGURE 9 | (Left) Full-field maps and (right) histogram of the distribution of the second harmonic phase Φ_D after applying the proposed corrective procedure. [Colour figure can be viewed at wileyonlinelibrary.com]

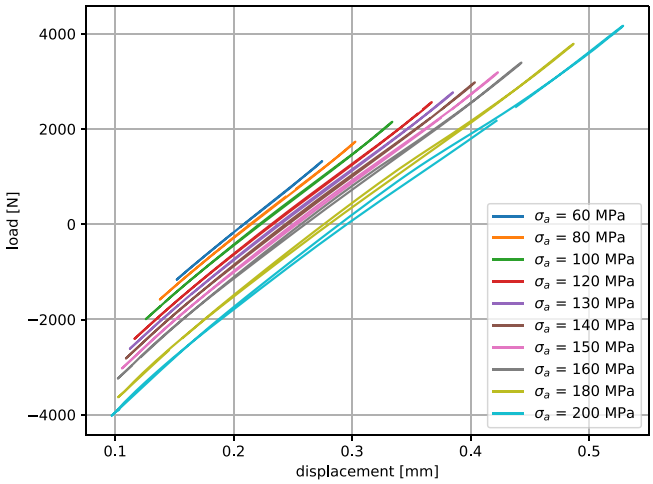

FIGURE 10 | Evolution of the hysteresis loops with different load-steps for specimen AL3. [Colour figure can be viewed at wileyonlinelibrary.com]

3.6 | Discussion

The proposed correction allowed for the isolation and extraction of information potentially linked to the onset of dissipative phenomena from the second harmonic of temperature. Before the correction, the second harmonic amplitude would provide misleading information about the onset of dissipation if not carefully decoupled of all competing effects and their phase information, which offers insights into the physical phenomena governing the material's behavior.

A comparison between Figures 4 and 9 demonstrates the effects of the proposed methodology on the phase of the second harmonic. In Figure 4, prior to correction, the second harmonic phase histograms exhibit a characteristic peak associated with the second-order thermoelastic effect at a phase value of 90°, which influence increases with the applied load amplitude. This peak is less relevant in the corrected data, as depicted in Figure 9. This is an interesting result and must be interpreted in conjunction with the amplitude of the second harmonic.

The decrease and convergence of the amplitude of the second harmonic in Figure 8 could be explained as follows: the magnitude of the dissipative heat source, which is opposite in phase to the second-order thermoelastic effect, is very low and hardly detectable for AL 2024 T3 [43]. Hence, the activation of such dissipative source is not able to drive the thermal response and cause the expected increase in amplitude due to the very high thermal diffusivity of the material. Instead, it manifests as a reduction of the second harmonic amplitude, buried in the second-order thermoelastic effect if the correction is not performed. If this interpretation is correct, the dissipative effect could be indirectly assessed, and further investigation is encouraged in this direction. Another interesting outcome, as analyzed in Section 2.6, is that the thermoelastic effect due to the second harmonic of the load signal appeared to reveal traces of dissipative behavior. The load cell exhibited a curious and peculiar second harmonic, consistent throughout the analyzed samples, indicating that the load signal might also contain valuable information about the material's behavior. It is worth to point out that deviations from the trends are found at the same stress levels in Figures 6 and 8, and reasonably close to values reported in the literature for the fatigue limit of this material ($\sigma_f = 138$ MPa [52]): This result is encouraging, but further studies are required to confirm this interpretation.

An analysis of the hysteresis loops, obtained by plotting displacements versus force of the load cell, could give additional information about the dissipative behavior of this material. As an example, Figure 10 compares the evolution of the hysteresis loops with different load steps for the sample AL3 (the same behavior has been encountered in all the tested specimens). The small areas of the hysteresis loops provides another qualitative evidence that supports the lack of onset of a marked dissipative behavior for this aluminum alloy: The low amount of dissipative heat produced would be immediately dispersed through the material due to its high thermal diffusivity. It is

here recalled the strong correlation between the dissipation codified in the second harmonic of temperature and the hysteresis loops [20, 25, 34].

In conclusion, the proposed correction appears to be promising in isolating traces of dissipative phenomena buried in the rich harmonic content of the second harmonic metric—that is, second-order thermoelastic effect and second harmonic of the load—potentially extending the application of rapid thermographic methods to materials with a strong higher order thermoelastic behavior.

4 | Conclusions

In this work, a framework for the detection of early dissipative phenomena in materials that exhibit non-negligible second order thermoelastic effects is proposed. Four nominally identical dogbone AL 2024 T3 specimens were tested with a loading ratio of $R = -1$, with the aim of detecting dissipative phenomena via a second harmonic Thermoelastic Stress Analysis. A range of different metrics has been analyzed, and a thorough investigation of the harmonic content of the load signal has been carried out.

The main conclusions of the investigation can be summarized as follows:

- It has been confirmed that the commonly used testing machines introduce an undesired second harmonic in the spectrum of the applied load. Given the typically low magnitude of the temperature second harmonic components, accounting for this effect provides more accurate estimations of the thermomechanical heat sources at twice the loading frequency.
- Materials that exhibit a pronounced second order thermoelastic effect produce a second harmonic component opposite in phase to the dissipation: This may results in a non-adiabatic behavior due to the proximity of points with a prevailing 2ω thermoelastic or 2ω dissipative components whose opposite phase determines strong local temperature gradients. This occurrence increases the difficulties in univocally identifying the stress level that leads to the onset of the dissipative behavior in the material.
- Experimental calibration of the second-order thermoelastic constant demonstrated remarkable agreement with literature values, providing an efficient indirect method to evaluate $\frac{\partial E}{\partial T}$.
- The evaluation of the mean temperature increase T_o presents a small deviation from linearity that can be correlated to the fatigue limit [8, 9], whereas the first harmonic amplitude did not aid in identifying dissipative phenomena onset.
- Prior to the application of the corrective methodology, the second harmonic amplitude D, and phase Φ_D are unable to provide any information about the onset of dissipation, showing a clear prevalence of the second-order thermoelastic effect.
- The proposed corrective procedure effectively identifies a bi-linear behavior in the second harmonic of temperature, which shows a convergence rather than an increase at a stress amplitude of 130 MPa. This unexpected behavior can be linked to the activation of the dissipative heat source; however, the intrinsic phase opposition to the second-order thermoelastic effect, together with the low magnitude of such dissipative heat source and the high thermal diffusivity of the material do not allow for the heat to develop and to be detected. This is further confirmed by the average phase of the second harmonic consistently approaching 0°, and the histograms corroborate the presence of the two antagonist phenomena.
- The first-order thermoelastic effect originated by the second harmonic of the load signal revealed some interesting features, suggesting the sensitivity of the testing machine's load cell to changes in material's behavior, that is, dissipation onset. Further studies are required to confirm this hypothesis.

The proposed methodology constitutes a significant step forward towards developing experimental protocols to identify fatigue dissipative phenomena for the important class of aluminum alloys, which are used in important industrial sectors such as aerospace and prosthetics, as well as for additive manufacturing applications. Similar outcomes are also expected for Titanium alloys, which are also renowned for their marked compliance with the second-order thermoelastic theory [42, 53].

Author Contributions

Riccardo Cappello: conceptualization, methodology, software, investigation, formal analysis, data curation, writing – original draft, visualization. **José Eugénio Semedo Garção:** methodology, data curation, writing – review and editing, resources. **Giuseppe Catalanotti:** conceptualization, methodology, formal analysis, writing – review and editing, resources, supervision. **Giuseppe Pitarresi:** conceptualization, methodology, formal analysis, writing – review and editing, resources, funding acquisition, supervision.

Acknowledgments

The first author acknowledges the support of the EPSRC Programme Grant "Certification for Design–Reshaping the Testing Pyramid" (CerTest, EP/S017038/1).

The IR thermal camera used in this work has been purchased using funds from the INTEP PO-FESR 2007/2013 4.1.2.A project awarded to the University of Palermo.

The signal processing methodology presented was developed with the support of the European Union's Framework Program for Research and Innovation – Mission 4 – Component C2 Investment 1.1 (PRIN - 2022) – project title MAdforLIFE, code: 2022JE3LRA_001, CUP: B53D23006070006.

Conflicts of Interest

The authors declare no conflicts of interest.

References

1. T. Boulanger, A. Chrysochoos, C. Mabru, and A. Galtier, "Calorimetric Analysis of Dissipative and Thermoelastic Effects Associated With the Fatigue Behavior of Steels," *International Journal of Fatigue* 26, no. 3 (2004): 221–229, https://doi.org/10.1016/S0142-1123(03)00171-3.

2. F. Maquin and F. Pierron, "Heat Dissipation Measurements in Low Stress Cyclic Loading of Metallic Materials: From Internal Friction to Micro-Plasticity," *Mechanics of Materials* 41, no. 8 (2009): 928–942.

3. A. Akai, D. Shiozawa, T. Yamada, and T. Sakagami, "Energy Dissipation Measurement in Improved Spatial Resolution Under Fatigue Loading," *Experimental Mechanics* 60 (2020): 181–189, https://doi.org/10.1007/s11340-019-00552-w.

4. M. Ricotta, G. Meneghetti, B. Atzori, G. Risitano, and A. Risitano, "Comparison of Experimental Thermal Methods for the Fatigue Limit Evaluation of a Stainless Steel," *Metals* 9, no. 6 (2019): 677, https://doi.org/10.3390/met9060677.

5. Z. Teng, "Thermo-Based Fatigue Life Prediction: A Review," *Fatigue & Fracture of Engineering Materials & Structures* 46, no. 9 (2023): 3121–3144.

6. M. Zaeimi, R. De Finis, D. Palumbo, and U. Galietti, "Fatigue Limit Estimation of Metals Based on the Thermographic Methods: A Comprehensive Review," *Fatigue & Fracture of Engineering Materials & Structures* 47, no. 3 (2024): 611–646, https://doi.org/10.1111/ffe.14206.

7. W. Wei, L. He, Y. Sun, and X. Yang, "A Review of Fatigue Limit Assessment Using the Thermography-Based Method," *Metals* 14, no. 6 (2024): 640.

8. M. P. Luong, "Fatigue Limit Evaluation of Metals Using an Infrared Thermographic Technique," *Mechanics of Materials* 28, no. 1-4 (1998): 155–163.

9. G. La Rosa and A. Risitano, "Thermographic Methodology for Rapid Determination of the Fatigue Limit of Materials and Mechanical Components," *International Journal of Fatigue* 22, no. 1 (2000): 65–73, https://doi.org/10.1016/S0142-1123(99)00088-2.

10. J. Krapez, D. Pacou, and G. Gardette, "Lock-In Thermography and Fatigue Limit of Metals," *Quant Infrared Thermogr* 5 (2000): 277–282, http://qirt.org/archives/qirt2000/papers/051.pdf.

11. C. Colombo, L. Vergani, and M. Burman, "Static and Fatigue Characterisation of New Basalt Fibre Reinforced Composites," *Composite Structures* 94, no. 3 (2012): 1165–1174, https://doi.org/10.1016/j.compstruct.2011.10.007.

12. R. De Finis, D. Palumbo, F. Ancona, and U. Galietti, "Fatigue Limit Evaluation of Various Martensitic Stainless Steels With New Robust Thermographic Data Analysis," *International Journal of Fatigue* 74 (2015): 88–96, https://doi.org/10.1016/j.ijfatigue.2014.12.010.

13. Q. Guo, X. Guo, J. Fan, R. Syed, and C. Wu, "An Energy Method for Rapid Evaluation of High-Cycle Fatigue Parameters Based on Intrinsic Dissipation," *International Journal of Fatigue* 80 (2015): 136–144, https://doi.org/10.1016/j.ijfatigue.2015.04.016.

14. D. Palumbo and U. Galietti, "Thermoelastic Phase Analysis (TPA): A New Method for Fatigue Behaviour Analysis of Steels," *Fatigue & Fracture of Engineering Materials & Structures* 40, no. 4 (2017): 523–534, https://doi.org/10.1111/ffe.12511.

15. D. Shiozawa, T. Inagawa, T. Washio, and T. Sakagami, "Accuracy Improvement in Dissipated Energy Measurement by Using Phase Information," *Measurement Science and Technology* 28, no. 4 (2017): 44004.

16. R. Urbanek and J. Bär, "Evaluation of the Thermo-Elastic Behavior of a High-Alloyed Steel by Fourier Transformation Based Lock-In-Thermography," in *Proceedings of QIRT 2018, 14th Quantitative Infrared Thermography Conference, 25–29 June 2018, Berlin, Germany*, (2018): 941–950, https://doi.org/10.21611/qirt.2018.127.

17. R. De Finis, D. Palumbo, M. M. Da Silva, and U. Galietti, "Is the Temperature Plateau of a Self-Heating Test a Robust Parameter to Investigate the Fatigue Limit of Steels With Thermography?," *Fatigue & Fracture of Engineering Materials & Structures* 41, no. 4 (2018): 917–934.

18. C. Colombo and L. Vergani, "Thermographic Applications for the Rapid Estimation of Fatigue Limit," *Procedia Structural Integrity* 24 (2019): 658–666.

19. C. Colombo, M. Sansone, L. Patriarca, and L. Vergani, "Rapid Estimation of Fatigue Limit for C45 Steel by Thermography and Digital Image Correlation," *Journal of Strain Analysis for Engineering Design* 56 (2020): 478–491, https://doi.org/10.1177/0309324720975284.

20. R. De Finis, D. Palumbo, and U. Galietti, "A Multianalysis Thermography-Based Approach for Fatigue and Damage Investigations of ASTM A182 F6NM Steel at Two Stress Ratios," *Fatigue & Fracture of Engineering Materials & Structures* 42, no. 1 (2019): 267–283, https://doi.org/10.1111/ffe.12903.

21. F. Giudice, G. La Rosa, G. Fargione, and R. Barbagallo, "Fatigue Limit Assessment by Energetic Analyses in Static and Cyclic Tensile Tests," *Procedia Structural Integrity* 24 (2019): 706–711.

22. S. Guo, X. Liu, H. Zhang, Z. Yan, Z. Zhang, and H. Fang, "Thermographic Study of AZ31B Magnesium Alloy Under Cyclic Loading: Temperature Evolution Analysis and Fatigue Limit Estimation," *Materials* 13, no. 22 (2020): 5209.

23. P. Corigliano, F. Cucinotta, E. Guglielmino, G. Risitano, and D. Santonocito, "Fatigue Assessment of a Marine Structural Steel and Comparison with Thermographic Method and Static Thermographic Method," *Fatigue and Fracture of Engineering Materials and Structures* 43, no. 4 (2020): 734–743, https://doi.org/10.1111/ffe.13158.

24. A. Lipski, "Change of Specimen Temperature During the Monotonic Tensile Test and Correlation Between the Yield Strength and Thermoelasto-Plastic Limit Stress on the Example of Aluminum Alloys," *Materials* 14, no. 1 (2021): 13, https://doi.org/10.3390/ma14010013.

25. G. Meneghetti and M. Ricotta, "Estimating the Intrinsic Dissipation Using the Second Harmonic of the Temperature Signal in Tension-Compression Fatigue: Part I. Theory," *Fatigue & Fracture of Engineering Materials & Structures* 44, no. 8 (2021): 2168–2185, https://doi.org/10.1111/ffe.13485.

26. R. De Finis, D. Palumbo, A. Pirinu, et al., "Fatigue Behaviour Assessment of C45 Steel by Means of Energy-Based Methods," in *Iop Conference Series: Materials Science and Engineering*, Vol. 1038. IOP Publishing, (2021): 12015.

27. R. Cappello, G. Meneghetti, M. Ricotta, and G. Pitarresi, "On the Correlation of Temperature Harmonic Content With Energy Dissipation in C45 Steel Samples Under Fatigue Loading," *Mechanics of Materials* 168 (2022): 104271.

28. A. Akai, Y. Sato, M. Murase, Y. Kojima, and Y. Okubo, "Rapid Determination of Fatigue Limit Using Temperature Second Harmonic," *Experimental Mechanics* 63, no. 2 (2023): 349–362.

29. R. Kawai, T. Yoshikawa, Y. Kurokawa, Y. Irie, and H. Inoue, "Rapid Evaluation of Fatigue Limit Using Infrared Thermography: Comparison Between Two Methods for Quantifying Temperature Evolution," *Mechanical Engineering Journal* 4, no. 5 (2017): 17–00009–17–00009, https://doi.org/10.1299/mej.17-00009.

30. W. P. Yang, J. L. Fan, Q. Guo, and X. L. Guo, "Experimental Procedure for Energy Dissipation Estimation During High-Cycle Fatigue Loading of Metallic Material," *Experimental Mechanics* 60 (2020): 695–712, https://doi.org/10.1007/s11340-020-00589-2.

31. G. Pitarresi and E. A. Patterson, "A Review of the General Theory of Thermoelastic Stress Analysis," *Journal of Strain Analysis for Engineering Design* 38, no. 5 (2003): 405–417.

32. G. Pitarresi, "Lock-In Signal Post-Processing Techniques in Infra-Red Thermography for Materials Structural Evaluation," *Experimental Mechanics* 55 (2015): 667–680, https://doi.org/10.1007/s11340-013-9827-1.

33. S. Quinn, J. M. Dulieu-Barton, and J. M. Langlands, "Progress in Thermoelastic Residual Stress Measurement," *Strain* 40, no. 3 (2004): 127–133.

34. N. F. Enke, "An Enhanced Theory for Thermographic Stress Analysis of Isotropic Materials," *Stress and Vibration: Recent Developments in Industrial Measurement and Analysis*, Vol. 1084, (1989): pp. 84–102.

35. R. De Finis, D. Palumbo, and U. Galietti, "On the Relationship Between Mechanical Energy Rate and Heat Dissipated Rate During Fatigue for a C45 Steel Depending on Stress Ratio," *Fatigue & Fracture of Engineering Materials & Structures* 44, no. 10 (2021): 2781–2799, https://doi.org/10.1111/ffe.13547.

36. G. Meneghetti and M. Ricotta, "Estimating the Intrinsic Dissipation Using the Second Harmonic of the Temperature Signal in Tension-Compression Fatigue. Part II: Experiments," *Fatigue & Fracture of Engineering Materials & Structures* 44, no. 8 (2021): 2153–2167, https://doi.org/10.1111/ffe.13484.

37. P. Bremond and P. Potet, "Lock-In Thermography: A Tool to Analyze and Locate Thermomechanical Mechanisms in Materials and Structures," in *Thermosense XXIII*, Vol. 4360. International Society for Optics and Photonics, (2001): 560–566.

38. R. De Finis, D. Palumbo, and U. Galietti, "Mechanical Behaviour of Stainless Steels Under Dynamic Loading: An Investigation With Thermal Methods," *Journal of Imaging* 2, no. 4 (2016), https://doi.org/10.3390/jimaging2040032.

39. R. Urbanek and J. Baer, "Influence of Motion Compensation on Lock-In Thermographic Investigations of Fatigue Crack Propagation," *Engineering Fracture Mechanics* 183 (2017): 13–25.

40. R. Barbagallo, G. Fargione, F. Giudice, and G. La Rosa, "Thermographic-DIC Approach in Fatigue Behaviour Analysis," in *Iop Conference Series: Materials Science and Engineering*, Vol. 1038. IOP Publishing, (2021): 12050.

41. D. Shiozawa, T. Inagawa, T. Washio, and T. Sakagami, "Fatigue Limit Estimation of Stainless Steels With New Dissipated Energy Data Analysis," *Procedia Structural Integrity* 2 (2016): 2091–2096, https://doi.org/10.1016/j.prostr.2016.06.262.

42. A. K. Wong, R. Jones, and J. G. Sparrow, "Thermoelastic Constant or Thermoelastic Parameter?," *Journal of Physics and chemistry of solids* 48, no. 8 (1987): 749–753.

43. A. E. Morabito, A. Chrysochoos, V. Dattoma, and U. Galietti, "Analysis of Heat Sources Accompanying the Fatigue of 2024 T3 Aluminium Alloys," *International Journal of Fatigue* 29, no. 5 (2007): 977–984.

44. A. Lipski and S. Mroziński, "The Effects of Temperature on the Strength Properties of Aluminium Alloy 2024-T3," *Acta Mechanica et Automatica* 6, no. 3 (2012): 62–66.

45. E. Astm, "Standard Test Methods for Tension Testing of Metallic Materials," (2001), Annual Book of ASTM Standards. ASTM.

46. J. Lemaitre and J.-L. Chaboche, *Mechanics of Solid Materials*, (Cambridge University Press, 1994).

47. A. Chrysochoos and H. Louche, "An Infrared Image Processing to Analyse the Calorific Effects Accompanying Strain Localisation," *International Journal of Engineering Science* 38, no. 16 (2000): 1759–1788.

48. V. Pinto, R. Cappello, S. Di Leonardo, G. Catalanotti, G. Burriesci, and G. Pitarresi, "Evaluation of NiTi Under Low-Amplitude Cyclic Loading by Means of Thermographic Harmonic Analysis," *Mechanics of Materials* 206 (2025): 105334, https://doi.org/10.1016/j.mechmat.2025.105334.

49. J. Eaton-Evans, J. M. Dulieu-Barton, E. G. Little, and I. A. Brown, "Thermoelastic Studies on Nitinol Stents," *Journal of Strain Analysis for Engineering Design* 41, no. 7 (2006): 481–495.

50. B. R. Boyce and J. R. Lesniak, "Thermoelastic Measurement Techniques Enabled by Self-Reference," *Conference Proceedings of the Society for Experimental Mechanics Series* 7 (2019): 125–127, https://doi.org/10.1007/978-3-319-95074-7_24.

51. G. Pitarresi, R. Cappello, and G. Catalanotti, "Quantitative Thermoelastic Stress Analysis by Means of Low-Cost Setups," *Optics and Lasers in Engineering* 134 (2020): 106158.

52. "Aluminum 2024-T3 Data Sheet on MatWeb,", [Online], accessed 09 December 2024, https://www.matweb.com/search/DataSheet.aspx?MatGUID%3D57483b4d782940faaf12964a1821fb61%26ckck%3D1.

53. A. K. Wong, J. G. Sparrow, and S. A. Dunn, "On the Revised Theory of the Thermoelastic Effect," *Journal of Physics and Chemistry of Solids* 49, no. 4 (1988): 395–400.